CD4^{+} T-cell epitope-based heterologous prime-boost vaccination potentiates anti-tumor immunity and PD-1/PD-L1 immunotherapy

Minglu Xiao,[1,2] Luoyingzi Xie,[1] Guoshuai Cao,[3] Shun Lei,[1,4] Pengcheng Wang,[5] Zhengping Wei,[1] Yuan Luo,[6] Jingyi Fang,[1] Xingxing Yang,[7] Qizhao Huang,[8] Lifan Xu,[1] Junyi Guo,[9] Shuqiong Wen,[9] Zhiming Wang,[1] Qing Wu,[1] Jianfang Tang,[1] Lisha Wang,[1] Xiangyu Chen,[8] Cheng Chen,[1] Yanyan Zhang,[10] Wei Yao,[1] Jianqiang Ye,[11] Ran He,[6] Jun Huang [ID],[3] Lilin Ye [ID] [1]

For numbered affiliations see end of article.

Correspondence to
Professor Lilin Ye;
yelilinlcmv@163.com

Professor Jun Huang;
huangjun@uchicago.edu

Professor Ran He;
ranhe@hust.edu.cn

Professor Jianqiang Ye;
jqye@yzu.edu.cn

ABSTRACT

Background Antitumor therapeutic vaccines are generally based on antigenic epitopes presented by major histocompatibility complex (MHC-I) molecules to induce tumor-specific CD8^{+} T cells. Paradoxically, continuous T cell receptor (TCR) stimulation from tumor-derived CD8^{+} T-cell epitopes can drive the functional exhaustion of tumor-specific CD8^{+} T cells. Tumor-specific type-I helper CD4^{+} T (T_H1) cells play an important role in the population maintenance and cytotoxic function of exhausted tumor-specific CD8^{+} T cells in the tumor microenvironment. Nonetheless, whether the vaccination strategy targeting MHC-II-restricted CD4^{+} T-cell epitopes to induce tumor-specific T_H1 responses can confer effective antitumor immunity to restrain tumor growth is not well studied. Here, we developed a heterologous prime-boost vaccination strategy to effectively induce tumor-specific T_H1 cells and evaluated its antitumor efficacy and its capacity to potentiate PD-1/PD-L1 immunotherapy.

Methods *Listeria monocytogenes* vector and influenza A virus (PR8 strain) vector stably expressing lymphocytic choriomeningitis virus (LCMV) glycoprotein-specific I-A^b-restricted CD4^{+} T cell epitope (GP_{61-80}) or ovalbumin-specific CD4^{+} T cell epitope ($OVA_{323-339}$) were constructed and evaluated their efficacy against mouse models of melanoma and colorectal adenocarcinoma expressing lymphocytic choriomeningitis virus glycoprotein and ovalbumin. The impact of CD4^{+} T cell epitope-based heterologous prime-boost vaccination was detected by flow-cytometer, single-cell RNA sequencing and single-cell TCR sequencing.

Results CD4^{+} T cell epitope-based heterologous prime-boost vaccination efficiently suppressed both mouse melanoma and colorectal adenocarcinoma. This vaccination primarily induced tumor-specific T_H1 response, which in turn enhanced the expansion, effector function and clonal breadth of tumor-specific CD8^{+} T cells. Furthermore, this vaccination strategy synergized PD-L1 blockade mediated tumor suppression. Notably, prime-boost vaccination extended the duration of PD-L1 blockade induced antitumor effects by preventing the re-exhaustion of tumor-specific CD8^{+} T cells.

Conclusion CD4^{+} T cell epitope-based heterologous prime-boost vaccination elicited potent both tumor-specific T_H1 and CTL response, leading to the efficient tumor control. This strategy can also potentiate PD-1/PD-L1 immune checkpoint blockade (ICB) against cancer.

INTRODUCTION

Tumor-infiltrating CD8^{+} T cells that specifically recognize tumor antigens undergo functional exhaustion due to prolonged antigen exposure and the suppressive microenvironment within tumor.[1] Exhausted tumor-specific CD8^{+} T cells progressively lose their effector functions and cytolytic capacity, concomitantly expressing high levels of inhibitory immune checkpoint receptors, such as PD-1, CTLA-4, TIM-3, and 2B4.[2] Immune checkpoint blockade (ICB) of these inhibitory receptors with monoclonal antibodies can reinvigorate exhausted tumor-specific CD8^{+} T cells in tumor microenvironment (TME),[3 4] laying the foundation of ICB to be used to treat cancer in the clinics.

ICB has demonstrated positive clinical outcomes in a wide variety of cancer types.[5–8] However, the response rate of ICB remains modest (about 20%–30%) and some malignancies, such as pancreatic adenocarcinoma and glioblastoma, are almost inert to respond to ICB.[8–12] Additionally, the adaptive resistance to ICB has become another challenge for achieving durable responses in patients with cancer.[13–15] The combination with other immunotherapy strategies, including therapeutic vaccines, has been considered to potentially optimize the efficacy of ICB in treating cancer.

Currently, cancer therapeutic vaccines mainly focus on augmenting the response

of tumor-specific CD8^{+} T cells by engaging major histocompatibility complex (MHC) class I restricted epitopes derived from tumor antigens. However, paradoxically, the strong T cell receptor (TCR) stimulation from high-loaded tumor-derived CD8^{+} T-cell epitopes may even exacerbate the exhaustion of tumor-specific CD8^{+} T cells.[16 17] In addition to tumor-specific CD8^{+} T cells, tumor-specific CD4^{+} T cells also play important roles in directly eliminating tumors or indirectly conferring essential help for supporting the tumoricidal function of tumor-specific CD8^{+} T cell population in TME.[18–20] In vivo depletion of CD4^{+} T cells promotes tumor progression while adoptive transfer of CD4^{+} T cells facilitates the repression of tumor growth.[21] Moreover, CD4^{+} T cells could also modulate TME by mediating cytokine and co-stimulatory signals.[18 22–24] Previous reports have also indicated that CD4^{+} T cells could optimize the priming of antitumor CD8^{+} T cells by educating dendritic cells.[25–27] Furthermore, the infiltration of tumor-reactive CD8^{+} T cells into TME could also be enhanced by CD4^{+} T cells.[28 29] Gene expression profiling has shown that the help from CD4^{+} T cells conferred CD8^{+} T cells more potent effector functions and less expression of inhibitory molecules compared with 'helpless' CD8^{+} T cells.[30] Tumor-specific type-I helper CD4^{+} T (T_H1) cells are believed to play primary roles in orchestrating direct antitumor immunity and indirectly coordinating tumor-specific CD8^{+} T cell response. Although these functionally important features of tumor-specific CD4^{+} T cells in antitumor immunity, the development of MHC class II-restricted epitopes as antitumor therapeutic vaccines draws less attention. It also remains largely unknown whether CD4^{+} T-cell epitope based therapeutic vaccines can potentiate or sustain antitumor effects of ICB.

Previously, we have designed a prime-boost vaccination with Listeria and influenza vectors that expressed a single LCMV-GP$_{61-80}$-specific CD4^{+} T cell epitope, which induced efficient anti-viral immunity against chronic LCMV-Cl13 infection in vaccinated mice.[31] To take advantage of this potent T_H1-biased induction system, here we engineered a murine melanoma cell line expressing LCMV glycoprotein (LCMV-GP) and examined the antitumor efficacy of this CD4^{+} T-cell epitope based immunization strategy. The antitumor effectiveness of combination of this vaccination strategy with ICB was also assessed.

MATERIALS AND METHODS
Mice, cell lines, bacteria and virus
The C57BL/6J mice (B6 mice) were purchased from The Jackson Laboratories. P14 and SMARTA mice were obtained from R. Ahmed, Emory University. All mice were bred in a specific-pathogen free facility. B16F10 melanoma cells (B16) and MC38 colon adenocarcinoma cells were purchased from ATCC. The B16F10 cell line expressing the glycoprotein of LCMV (B16-GP) was generated by CRISPR/Cas9-mediated insertion (Beijing Biocytogen Co.Ltd). B16F10 melanoma cells and MC38

colon adenocarcinoma cells stably expressing membrane-bound ovalbumin(OVA) (B16-OVA; MC38-OVA) were generated by transfecting with pCl-neo-mOVA plasmid (Addgene, 25099) and then selected by 1 mg/mL G418 (Invivogen) for 2 weeks.

Listeria monocytogenes expressing LCMV glycoprotein-specific I-A[b]-restricted CD4^{+} T cell epitope GP$_{61-80}$ (LM-GP61) was purchased from Biources.[32] *Listeria monocytogenes* expressing melanoma associated antigen tyrosinase-related protein 1 (TRP-1) specific CD4^{+} T cell epitope TRP-1$_{106-130}$ or ovalbumin-specific CD4^{+} T cell epitope OVA$_{323-339}$ were constructed as LM-GP61.[32] Influenza A virus (PR8 strain) expressing LCMV GP$_{61-80}$ (IAV-GP61) was constructed as previously described.[31] Influenza A virus (PR8 strain) expressing melanoma associated antigen tyrosinase-related protein 1 (TRP-1) specific CD4^{+} T cell epitope TRP-1$_{106-130}$ or ovalbumin-specific CD4^{+} T cell epitope OVA$_{323-339}$ (IAV-OVA$_{323-339}$) were similarly prepared as IAV-GP61.[31]

All immunized mice were housed in accordance with institutional biosafety regulations of Third Military Medical University. All mouse experiments were performed according to the guidelines of the Institutional Animal Care and Use Committees of Third Military Medical University.

LD50 measurement
Before determining the lethal dose, we first titrated IAV vector by TCID50. At first, MDCK cells were seeded in 96-well plates and then infected with 10-fold serially diluted IAV-OVA$_{323-339}$, IAV-GP$_{61-80}$ or IAV-TRP-1$_{106-130,}$ which were originally propagated on specific-pathogen-free eggs. After 1 day, we recorded the cytopathic cells and calculated the TCID50.[33] To calculate the lethal dose (LD), 8-week-old C57BL/6 mice were divided into six groups and infected with 10^1–10^6 TCID50 viruses intranasally. Lethal dose calculation was determined based on mortality. In our study, 0.5 LD50 of IAV-OVA$_{323-339}$ (about 1400 TCID50), IAV-GP$_{61-80}$ (about 2500 TCID50) and IAV-TRP-1$_{106-130}$ (about 2000 TCID50) were used.

Tumor implantation, tumor volume and weight measurements
Mice at 6–10 weeks of age were inoculated subcutaneously (s.c) with 1×10^6 tumor cells at the right lower flank unless otherwise indicated. Tumor volumes were measured in two dimensions using a caliper and calculated by the formula (length × width^2/2). Mice were sacrificed when tumor volumes reached 2000 mm^3 and the weight of the excised tumor was determined.

Adoptive transfer
To deplete endogenous T cells for the optimal efficiency of adoptively transferred T cells with transgenic TCRs, cyclophosphamide (CTX) was administered intraperitoneally (i.p) with a dose of 200 mg/kg. For adoptive transfer, 1×10^6 P14 (CD45.1^{+}) cells or SMARTA (CD45.1^{+}) cells from donor mice were injected intravenously into the recipient mice 24 hours post-CTX manipulation.

Lung and liver metastasis

To establish the lung metastasis model, 3×10^5 B16-GP cells in 500 µL phosphate-buffered saline (PBS) were injected intravenously into the circulation of mice through their tail veins. To induce the development of liver metastasis, mice were injected intrasplenically with 5×10^5 B16-GP cells in 50 µL of PBS, followed by splenectomy at 3 min after injections.

Isolation of tumor infiltrating lymphocytes

Isolated tumors were cut into small pieces (1–2 mm) and digested in the buffer which composed of RPMI-1640 medium (Sigma-Aldrich) and 1 mg/mL collagenase type IV (Sigma-Aldrich), collagenase type II (Sigma-Aldrich) or collagenase type I (Sigma-Aldrich)[34 35] and incubated 45 min at 37°C in a shaking incubator (Eppendorf New Brunswick Excella E25) at 200 rpm. The digested tumor pieces then filtered through 100 µm strainers and immune cells were enriched by using Percoll density gradient centrifugation suspended in 40% Percoll, layered on top of 60% Percoll and centrifuged at 900 g for 30 min at room temperature without brake. Cells at the interface of the two Percoll layers were harvested and subsequently washed with FACS buffer in preparation for antibody staining.

Flow cytometry and antibodies

The following antibodies were used: anti-CD8α (Biolegend, clone 53-6.7), anti-CD4 (Biolegend, clone RM4-5), anti-CD44 (Invitrogen, clone IM7), anti-CD45.1 (Biolegend, clone A20), anti-PD-1 (Biolegend, clone 29F.1A12), anti-IFN-γ (BD Biosciences, clone XMG1.2), anti-TNF-α (BD Biosciences, clone MP6-XT22), anti-CD11b (Biolegend, clone M1/70), anti-CD4 (Biolegend, clone RM4-5), anti-CD8 (Biolegend, clone 53–6.7), anti-CD11c (Biolegend, clone N418), anti-MHCII (Biolegend, clone AF6-120.1), anti-CD103 (Biolegend, clone 2E7). MHC class I peptide tetramers of the LCMV GP_{33-41} were obtained from R. Ahmed, Emory University. For the surface staining, PBS containing 2% BSA or FBS (wt/vol) was used. For intracellular cytokine staining, the tumor infiltrating lymphocytes (TILs) were first stimulated with the LCMV GP_{33-41} and B16F10 GP_{100} peptides (0.2 µg/mL) or Phor- bol-12-myristat-13-acetat (PMA) (40 ng/mL) plus Ionomycin (400 ng/mL) for 5 hours in the presence of Brefeldin A (7 mg/mL) and then performed using a Cytofix/Cytoperm Fixation/Permeabilization Kit (BD Biosciences, 554714) according to the manufacturer's instructions.[31] The samples were collected by a FACSCanto II (BD Biosciences) flow cytometer or BD LSRFortessa (BD Biosciences) and analyzed by FlowJo (Treestar). Cell sorting was performed with a FACS Aria III (BD Biosciences).

Vaccination and in vivo antibody blockade

For B16-GP tumor model, the tumor bearing mice were immunized with 1×10^6 CFU of LM-GP61, and then with 0.5 LD50 (50% lethal dose) IAV-GP61. For B16-OVA and MC38-OVA tumor model, the mice were immunized with 1×10^6 CFU of Listeria-$OVA_{323-339}$ and 0.5 LD50 (50% lethal dose) IAV-$OVA_{323-339}$ sequentially. The immunization was injected intraperitoneally (i.p) or subcutaneously (s.c).

For the PD-L1 blockade, 200 µg rat anti-mouse PD-L1 antibody (PD-L1 mAb) (BioXcell, 10F.9G2) was administered (i.p).

To deplete CD8+ T or CD4+ T cells, mice were injected intra-peritoneally with 200 µg rat anti-mouse CD8 antibody (CD8 mAb) (BioXcell, YTS 169.4) or 200 µg rat anti-mouse CD4 antibody (GK1.5 mAb) (BioXcell, GK1.5) on day 1, 2, 7 and 12.

Resection assay

The tumors were surgically resected when the tumor volume reached 75 mm^3. The mice were then randomly divided into two groups. One group received prime-boost vaccination treatment while the other received PBS as control.

Single-cell RNA sequencing and single-cell TCR sequencing

Cellular suspensions were loaded on a 10X Genomics GemCode Single-cell instrument that generates single-cell Gel Bead-In-EMlusion (GEMs) with Chromium Next GEM Single Cell 5' Reagent Kits v2 (PN-1000263). The expression libraries were generated from the half of cDNAs with Library Construction Kit (PN-1000190) and the TCR libraries were constructed with the other half cDNAs by Chromium Single Cell Mouse TCR Amplification Kit (PN-1000254). Both of the libraries were sequenced using Illumina Novaseq6000 by Gene Denovo Biotechnology Co (Guangzhou, China).

Single-cell RNA-seq data processing

The scRNA-seq reads were aligned to the mm10 reference genome and quantified using the cellranger count (10X Genomics, V.3.0.0). The filtered gene-barcode matrices with unique molecular identifier counts that passed the quality control were proceeded for downstream analyses. We obtained a total of 20 062 cells from 3 samples with on average 65 315 reads per cell and a median of 1579 genes per cell.

UMAP analysis and clustering on single-cell RNA-seq data

UMAP analysis and clustering were performed using the Seurat package (V.3.1.2).[36] Raw count matrices from three samples were first converted to Seurat object before further merged into one Seurat object. Following that, cells with less than 200 genes detected or greater than 25% mitochondrial RNA content were excluded from further analysis, with 19 954 retained after filtering.

Then, the NormalizeData function with default options was used to log-normalize the raw counts. Top 5000 variable features were then characterized using the FindVariableFeatures function with the default 'vst' method. The data were then centered and scaled using the ScaleData function, with additional regression against the percent of mitochondrial RNA content and cell cycle scores calculated using CellCycleScoring function. Scaled data

were then used as input for principal component analysis (PCA) on the basis of variable genes using the RunPCA function. UMAP was then constructed based on the first 30 principal components, with 'n.neighbors=15' and 'min.dist=0.1'. The same principal components were then used to construct the shared nearest neighbor (SNN) graph using the FindNeighbors function, which was then partitioned to identify clusters using the FindClusters function with default Louvain algorithm and 'resolution=0.3'. These clusters were then manually aggregated and classified into 'Non-T', 'CD4', 'CD8' (2275, 6488, 11 191 cells, respectively) based on each cluster's expression of Cd3g, Cd3d, Cd3e, Cd4, Cd8a, and Cd8b1. The 'Non-T' cells were then removed, and the 'CD4' and 'CD8' cells were then re-analyzed separately with the same steps as above starting from redoing normalization. The only differences were: (1) top 50 PCs were used for both cases; (2) for clustering, resolution parameters used were 0.7 for CD4 T cells and 0.3 for CD8 T cells; (3) for UMAP construction, neighbors were set to be 15 for CD4 T cells and 20 for CD8 T cells. Subsets of CD4 and CD8 T cells were annotated based on the selectively up-regulated gene markers in each cluster according to published literatures.[37–41]

Differential gene expression analysis on single-cell RNA-seq data

Differential gene expression analyses were all performed using the FindMarkers function in Seurat (V.3.1.2) package, with default parameters and the appropriate 'ident.1' and 'ident.2' set as contrast. Unless otherwise stated, the results were then filtered with p_val_adj<0.05 and abs(avg_logFC)>0.25.

Single-cell TCR-seq data processing and analysis

The scTCR-seq reads were aligned to the 10× curated GRCm38 vdj reference genome and quantified using the cellranger vdj (10× Genomics, V.3.0.0). The resultant clonotype and filtered contig annotation data were used for downstream analyses. The clonotype and contig data were then added to the scRNA data by matching the cell barcodes. The frequency of each clonotype in each sample was recalculated based on those successfully matched to the corresponding scRNA data. An overall frequency of each clonotype was also calculated by pooling all clonotypes from the Naïve, Control and Vaccine data and then recalculating. The above analyses were done for CD4 and CD8 separately.

Plots

Unless otherwise stated, all plots were constructed in R (V.3.6.1) using ggplot2 (V.3.2.1).

Statistical analysis

The statistical analysis was conducted using Prism V.8.4.0 (GraphPad). Statistical differences were assessed by a two-tailed unpaired Student's t-test with a 95% CI and ordinary one-way analysis of variance (ANOVA) analysis. Statistical differences in the Kaplan-Meier survival curve

were assessed by a Mantel-Cox log-rank test. Statistical significance for tumor growth was determined by two-way ANOVA, *p<0.05, **p<0.01, ***p<0.001, ****p<0.0001, ns stands for not significant. Results were presented as mean±SEM unless otherwise indicated.

RESULTS

CD4^{+} T cell epitope-based heterologous prime-boost vaccination efficiently inhibited tumor growth in immunized mice

To probe the antigenicity and prophylactic effect of the CD4^{+} T-cell epitope-based vaccination against tumors, we first primed C57BL/6 (B6) mice with *Listeria monocytogene* vector that expressed the LCMV glycoprotein-specific I-A^b-restricted CD4^{+} T cell epitope $GP_{61–80}$(LM-GP61) on Day 0 followed by boosting the primed mice 7 days later with an influenza A virus (PR8 strain) vector that expressed the same CD4^{+} T cell epitope (IAV-GP61). Subsequently, mice were inoculated subcutaneously with B16F10 melanoma cells expressing LCMV glycoprotein (B16-GP) (figure 1A). We observed that mice received the vaccination showed significantly limited tumor growth and better survival in comparison with control mice (figure 1B), suggesting that this single CD4^{+} T-cell epitope-based vaccination strategy was immunogenic and could induce potent antitumor immunity in naïve mice. Next, we assessed the therapeutic capacity of this vaccination on tumor bearing mice. We used this prime-boost strategy to immunize B6 mice on early (day 5) stage post-tumor inoculation (figure 1C). Early immunized tumor-bearing mice exhibited greatly reduced tumor progression and substantially improved the survival rate compared with non-immunized controls (figure 1D). Subsequently, we investigated the effect of this vaccination strategy in the inhibition of tumor growth at advanced stage of tumor progression (figure 1E). To this end, we vaccinated the mice when tumors grew up to 75 mm^3(on day 9 post-B16-GP inoculation). Likewise, the vaccination significantly inhibited the tumor growth and increased the survival rate in immunized animals compared with control animals at the advanced stage (figure 1F). Notably, the prime-boost vaccination strategy with LM-OVA$_{323-339}$ (*Listeria monocytogenes* expressing ovalbumin-specific CD4^{+} T cell epitope OVA$_{323-339}$) and IAV-OVA$_{323-339}$ (Influenza A virus expressing ovalbumin-specific CD4^{+} T cell epitope OVA$_{323-339}$) could also efficiently curtail tumor growth of B16F10 cell line expressing OVA (B16-OVA) (online supplemental figure S1A-C) and mouse colorectal adenocarcinoma cell line MC38 expressing OVA (MC38-OVA) (online supplemental figure S1D), which generalized this strategy to other tumor-specific CD4^{+} T cell epitopes and tumor types. These results demonstrated that exogenous CD4^{+} T cell epitope-based prime-boost vaccination exhibited strong suppression of tumor growth. To investigate whether endogenous CD4^{+} T cell epitopes can also be effective in suppressing tumor growth when inserted into IAV and LM vectors, we inoculated C57BL/6 mice with
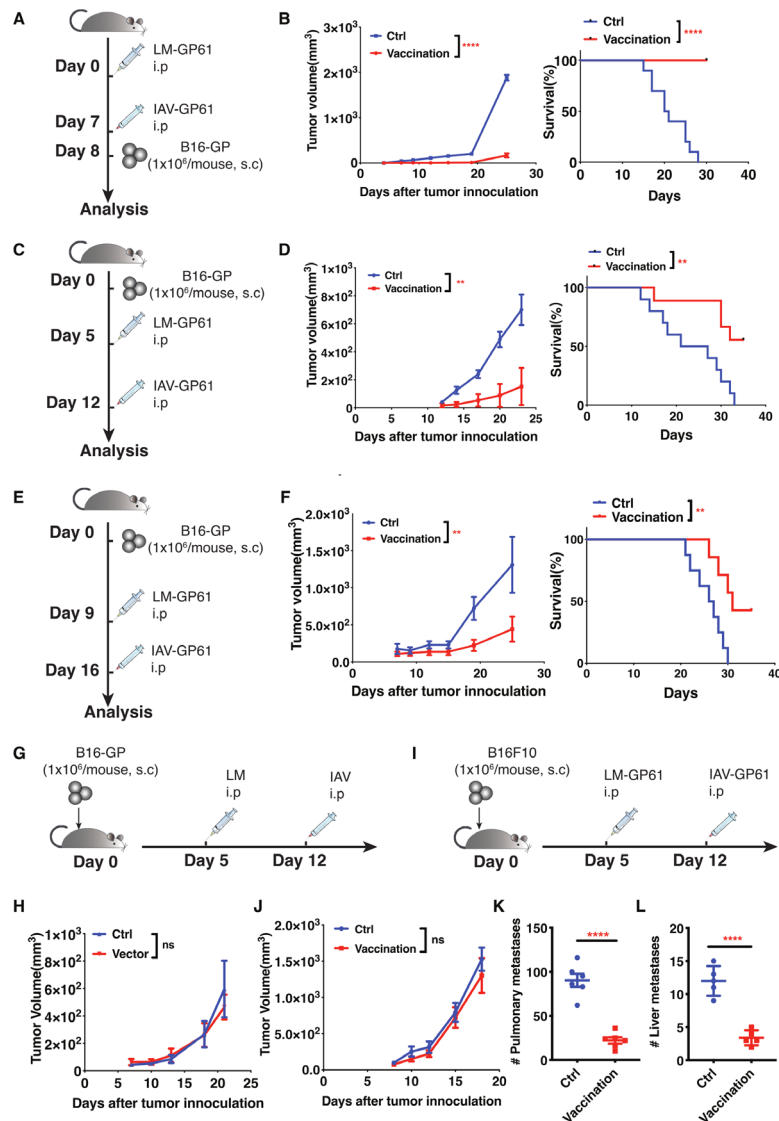
Figure 1 CD4+ T cell epitope-based heterologous prime-boost vaccination efficiently inhibits tumor growth in immunized mice. (A) Experimental design for examining prophylactic effect of prime-boost vaccination on syngeneic tumor transplantation. C57BL/6 mice (B6 mice) were immunized intraperitoneally (i.p) with LM-GP61(1×10^6 CFU) and IAV-GP61(0.5 LD50) on day 0 and day 7, respectively. The mice were then inoculated subcutaneously (s.c) with B16-GP (1×10^6 cells/mouse) on day 8 and allowed to grow until analysis. (B) Tumor growth (ctrl, n=5; vaccination, n=4) and the Kaplan-Meier survival curve (ctrl, n=10; vaccination, n=9) of prophylactically vaccinated mice (vaccination) and control mice (ctrl) in syngeneic transplantation. Tumor volumes were measured every 3–7 days. (C) Experimental design for examining therapeutic effect of prime-boost vaccination on early-stage tumor. B6 mice were inoculated with B16-GP (1×10^6 cells/mouse, s.c) on day 0 and then received LM-GP61 (1×10^6 CFU) and IAV-GP61 (0.5 LD50) on day 5 and day12, respectively. (D) Tumor growth (Ctrl, n=5; vaccination, n=6) and the Kaplan-Meier survival curve (ctrl, n=10; vaccination, n=9) of vaccinated mice (vaccination) and control mice (ctrl) with an early-stage immunization. Tumor volumes were measured every 3 or 4 days. (E) Experimental design for examining therapeutic effect of prime-boost vaccination on advanced-stage tumor. B6 mice were inoculated with B16-GP (1×10^6 cells/mouse, s.c) on day 0 and then received LM-GP61 (1×10^6 CFU) and IAV-GP61 (0.5 LD50) on day 9 and day 16, respectively. (F) Tumor growth (ctrl, n=5; vaccination, n=6) and the Kaplan-Meier survival curve (ctrl, n=8; vaccination, n=7) of vaccinated mice (vaccination) and control mice (ctrl) with an advanced-stage immunization. Tumor volumes were measured every 3–7 days. (G) B16-GP tumor-bearing mice were injected with Listeria (1×10^6 CFU) and IAV (0.5 LD50) without expressing LCMV GP$_{61-80}$.Tumor growth (ctrl, n=5; vector, n=10) is shown in (H). Tumor volumes were measured every 3–6 days. (I) B6 mice inoculated with B16 tumor cells (1×10^6 cells/mouse, s.c) without expressing GP were injected i.p with LM-GP61 and IAV-GP61 at indicated time points. Tumor growth (n=5) is shown in (J). Tumor volumes were measured every 3 or 4 days. (K) B6 mice were injected B16-GP tumor cells intravenously into the circulation of mice to set up lung metastasis model and received vaccination on day 3 and day 10. (n=6) (L) B6 were injected with B16-GP tumor cells, followed by splenectomy at 3 min after injections to set up liver metastasis model and received vaccination on day 1 and day 8 (n=5). Statistical differences are assessed by a two-tailed unpaired Student's t-test (K, L), a Mantel-Cox log-rank test for the Kaplan-Meier survival curve and two-way ANOVA (analysis of variance) for tumor growth. **P<0.01, ****p<0.0001, ns stands for not significant. Error bars (B, D, F, H, J, K, L) denote SEM. All data are representation of two independent experiments.

B16F10 and then treated with *Listeria monocytogene* and influenza A virus expressing an endogenous CD4$^+$ T cell epitope derived from melanoma associated antigen tyrosinase related protein (TRP-1), TRP-1$_{106-130}$ on day 5 and day 12, respectively. We found that, consistent with exogenous GP$_{61-80}$ epitope, tumor-associated endogenous TRP-1 specific CD4$^+$ T cell epitope (TRP-1$_{106-130}$) based prime and boost immunization also induced substantial tumor growth inhibition (online supplemental figure 1E–F), illuminating that endogenous CD4$^+$ T cell epitopes are also applicable to heterologous prime-boost immunization strategy.

The inhibition of tumor growth was attributable to the integrated prime and boost vaccination, since we found that immunization of B16-GP bearing mice with either LM-GP61 or IAV-GP61 alone did not efficiently diminish the tumor volumes (online supplemental figure 1G,H). Furthermore, the order of vectors used in prime and boost did not fundamentally influence the efficacy of our immunization strategy in the inhibition of tumor growth (online supplemental figure 1I–J). Both LM and IAV vectors have been reported to induce certain levels of antitumor therapy.[42–45] To rule out the antitumor effects of vector itself, we immunized tumor-bearing mice with empty LM and IAV vectors. We noted comparable tumor growth between control and vaccinated mice (figure 1G,H), highlighting the importance of tumor-derived CD4$^+$ T cell epitopes contained in these vectors in the control of tumor progression. To further confirm this note, we inoculated mice with B16F10 tumor cells (B16) without expressing LCMV GP and then primed the mice with LM-GP61 and boosted by IAV-GP61. As expected, this vaccination did not effectively inhibit tumor growth in B16F10 engrafted mice (figure 1I,J).

Tumor metastasis and postsurgery tumor recurrence have long been clinical conundrums. We found that prime-boost immunization with LM-GP61 and IAV-GP61 was able to profoundly reduce metastatic loci in both lung and liver B16-GP metastases (figure 1K and L). Next, to investigate whether the vaccination could prevent postsurgery tumor recurrence, we administered mice with prime (LM-GP61)-boost (IAV-GP61) vaccination after B16-GP tumor resection and observed this vaccination could also greatly inhibit tumor relapse (online supplemental figure 2A,B). To evaluate whether different routes of administration would affect efficacy of this prime-boost vaccination strategy, we also vaccinated tumor-bearing mice subcutaneously. We found that giving prime-boost vaccination subcutaneously also remarkably blocked the tumor growth (online supplemental figure 2C). Taken together, these results demonstrated that prime-boost immunization strategy with tumor-derived CD4$^+$ T cell epitope based vaccines was able to efficiently inhibit tumor progression, metastasis and postsurgery tumor recurrence.
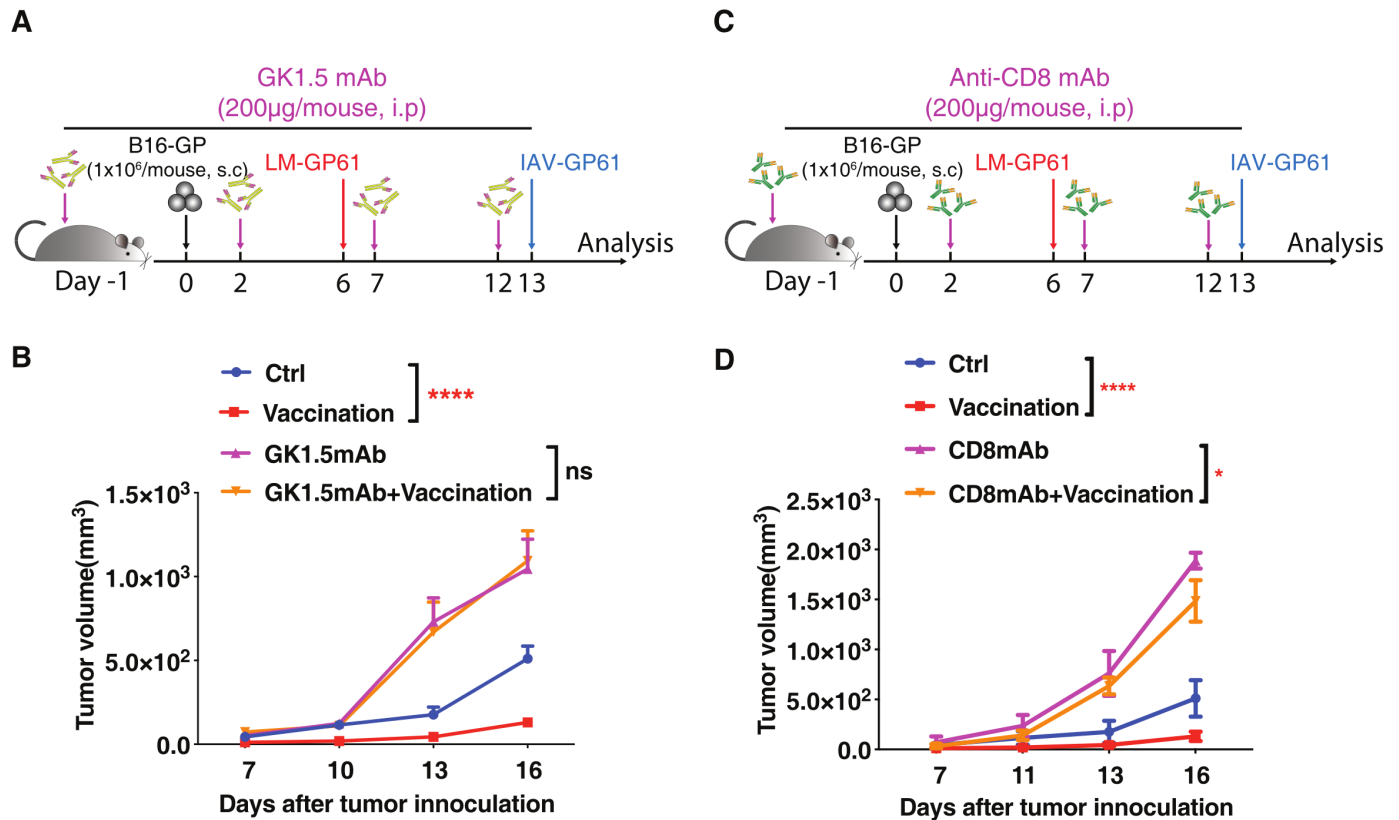
Both CD4$^+$ and CD8$^+$ T cells response induced by vaccination are essential for suppressing tumor growth

To determine whether CD4$^+$ T cells or CD8$^+$ T cells were responsible for preventing tumor growth after prime-boost immunization with LM-GP61 and IAV-GP61 sequentially, we subcutaneously inoculated B16-GP tumor cells and treated CD4$^+$ T cell or CD8$^+$ T cell depletion with specific monoclonal antibodies in B6 mice (figure 2A,C). These tumor-bearing mice were then primed and boosted on day 6 and day 13 post-tumor inoculation (figure 2A,C). As expected, the depletion of either CD4$^+$ T cells or CD8$^+$ T cells abrogated the therapeutic effect of the vaccination (figure 2B,D), highlighting that the antitumor efficacy of the vaccination was strictly depended on both CD4$^+$ T cells and CD8$^+$ T cells.

Tumor infiltrating CD4$^+$ T cells induced by the prime-boost vaccination tend to be T$_H$1-polarized

To interrogate the molecular characteristics of CD4$^+$ T cell induced by prime-boost vaccination with LM-GP61 and IAV-GP61, we performed single-cell RNA-sequencing and single-cell TCR-sequencing on CD4$^+$ T cells from tumors of control and vaccinated mice, and CD4$^+$ T cells from lymph nodes of naïve mice as a control. We found that the CD4$^+$ T cells in vaccination group expressed highest levels of effector and cytolytic molecules, such as *Tnf, Ifng, Gzmb and Gzmk* than other groups. Moreover, CD4$^+$ T cells in vaccination group also increased expression level of *Tbx21*, the master transcription factor governing T$_H$1 cell differentiation (figure 3A). Data integration revealed that CD4$^+$ T cells from distinct groups were prominently different from each other, although few cells from the control tumor group were close to the vaccination group (figure 3B). Subclustering of CD4$^+$ T cells by four clusters showed that the majority of CD4$^+$ T cells from vaccinated mice were T$_H$1-type cells (figure 3C,D), displaying high expression levels of *Ifng* and *Tbx21* (figure 3E). By single-cell TCR analysis, we found that most of the top20 clonally expanded TCRs were located in vaccinated mice and belonged to the T$_H$1 cells (figure 3F,G), illustrating that T$_H$1 cells in TME from vaccinated tumor-bearing mice were clonally expanded in response to prime-boost immunization.

To further confirm the functional status of vaccination-induced CD4$^+$ T cells in tumor bearing mice, we next evaluated the expression of effector markers on SMARTA CD4$^+$ T cells bearing a transgenic TCR for LCMV GP$_{61-80}$, which were transferred to tumor-bearing mice before vaccination. We found that TNF-α and IFN-γ coexpression was significantly upregulated in SMARTA cells from tumor-bearing mice with vaccination compared with non-vaccinated tumor-bearing mice (figure 3H,I), demonstrating prime-boost vaccination strategy with CD4$^+$ T cell epitope could induce the differentiation of epitope specific T$_H$1 cells with potent polyfunctionality.

Figure 2 Both CD4+ and CD8+ T cells responses induced by the vaccination are essential for suppressing tumor growth. (A) Experimental design for CD4+ T cells depletion during vaccination in syngeneic tumor transplantation. B6 mice were received anti-CD4+ T cell monoclonal antibody GK1.5 mAb (200 µg/mouse, intraperitoneally) at indicated time points during an entire vaccination process in syngeneic tumor transplantation as scheme shown. (B) Tumor volumes of vaccinated mice and control mice with or without GK1.5 mAb. Tumor volumes were measured every 3 or 4 days (n=6, ctrl, vaccination; n=5, GK1.5 mAb, GK1.5 mAb +vaccination). (C)Experimental design for CD8+ T cells depletion during vaccination in syngeneic tumor transplantation. B6 mice were received anti-CD8+ T cell monoclonal antibody (CD8 mAb) (200 µg/mouse, intraperitoneally) at indicated time points during an entire vaccination process in syngeneic tumor transplantation as scheme shown. (D) Tumor volumes of vaccinated mice and control mice with or without CD8 mAb. Tumor volumes were measured every 3 or 4 days (n=6, ctrl, vaccination; n=5, CD8 mAb, CD8 mAb +vaccination). Statistical significance for tumor growth (B, D) are determined by two-way ANOVA. *P<0.05, ****p<0.0001 and ns stands for not significant. Error bars (B, D) denote SEM. Data are representation of two (A–D) independent experiments. ANOVA, analysis of variance.

The prime-boost vaccination induced strong tumor-specific CD8+ T cell response

Tumor-specific CD8+ T cells are known to be essential to constrain tumor growth. To investigate the effect of the prime-boost vaccination with CD4+ T cell epitope on CD8+ T cells, we compared the frequency and number of tumor-infiltrated CD8+ T cells in vaccinated and control mice bearing B16-GP melanoma. It turned out that vaccination significantly increased the percentage and number of bulk CD44hiCD8+ T cells infiltrated in TME (figure 4A), as well as antigen-specific tetramer-positive CD8+ T cells (figure 4B). To assess the effector function of tumor-specific CD8+ T cells, we next stimulated these cells with tumor-derived peptides in vitro and measured the expression level of IFN-γ produced by these CD8+ T cells. We observed that CD8+ T cells in TME of vaccinated tumor-bearing mice exhibited more abundance of IFN-γ than the counterparts in non-vaccinated tumor-bearing mice (figure 4C). Collectively, these results revealed that a
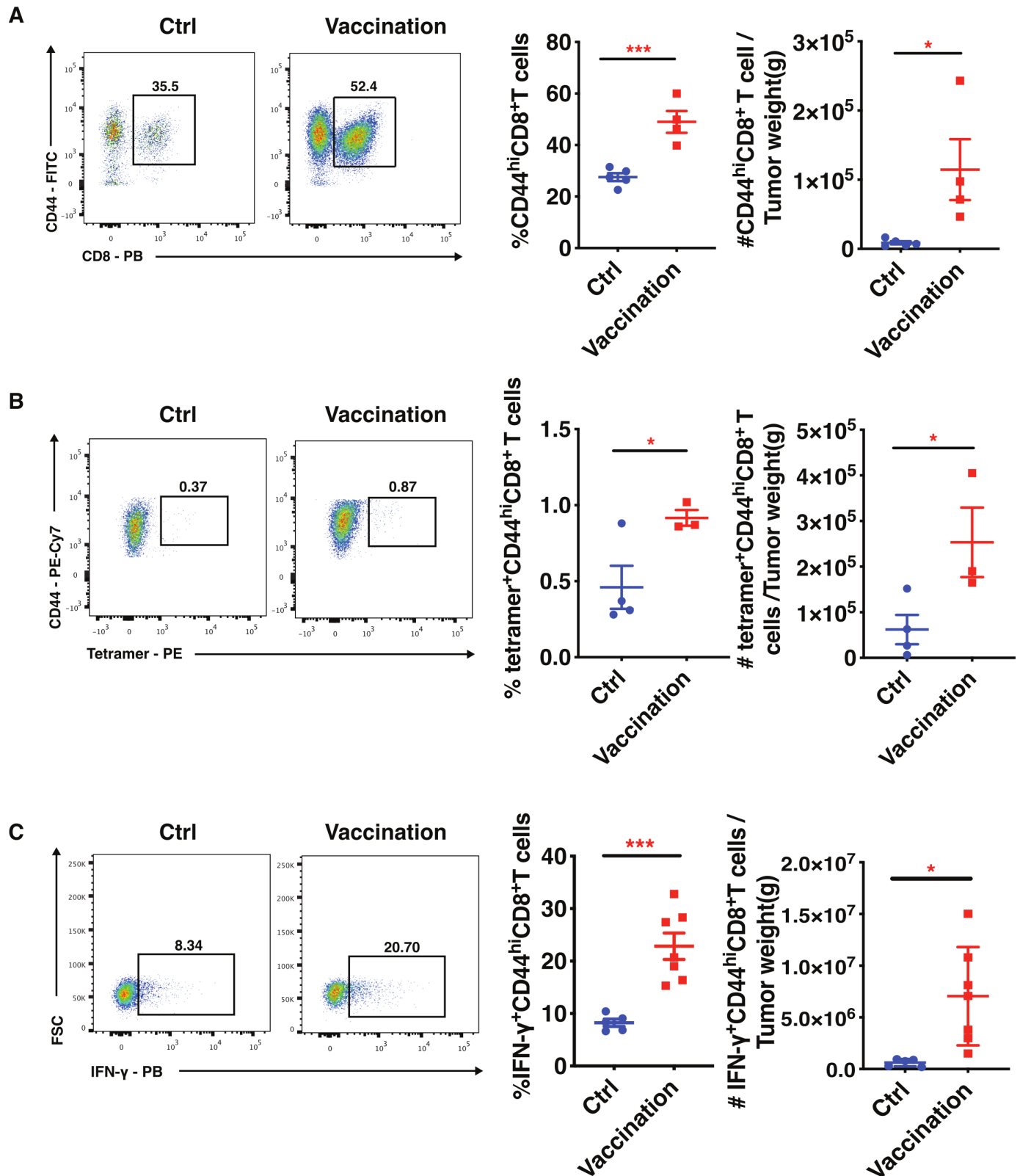
single CD4+ T cell epitope-based prime-boost vaccination can effectively induce tumor-specific CD8+ T cell response.

As the prime-boost vaccination induced potent antigen-specific CD8+ T cell response, which resulted in a complete remission in a fraction of mice (figure 1C–F), we speculated whether immune memory towards tumors has been established in these tumor-free mice. We then rechallenged vaccination cured tumor-free mice with B16-GP cells and found that all of these mice had no obvious tumor growth and could survive the second challenge (online supplemental figure 3A-C). To further confirm this immune memory is tumor-specific, we rechallenged the vaccinated tumor-free mice with MC38 tumor cells or B16F10 tumor cells (online supplemental figure 3D). As expected, a part of tumor-free mice which were re-challenged with B16F10 tumors were protected from tumor again, however, all of the B16-GP tumor-free mice re-challenged with MC38 tumors succumbed to death, indicating the immune memory formed by prime-boost vaccination
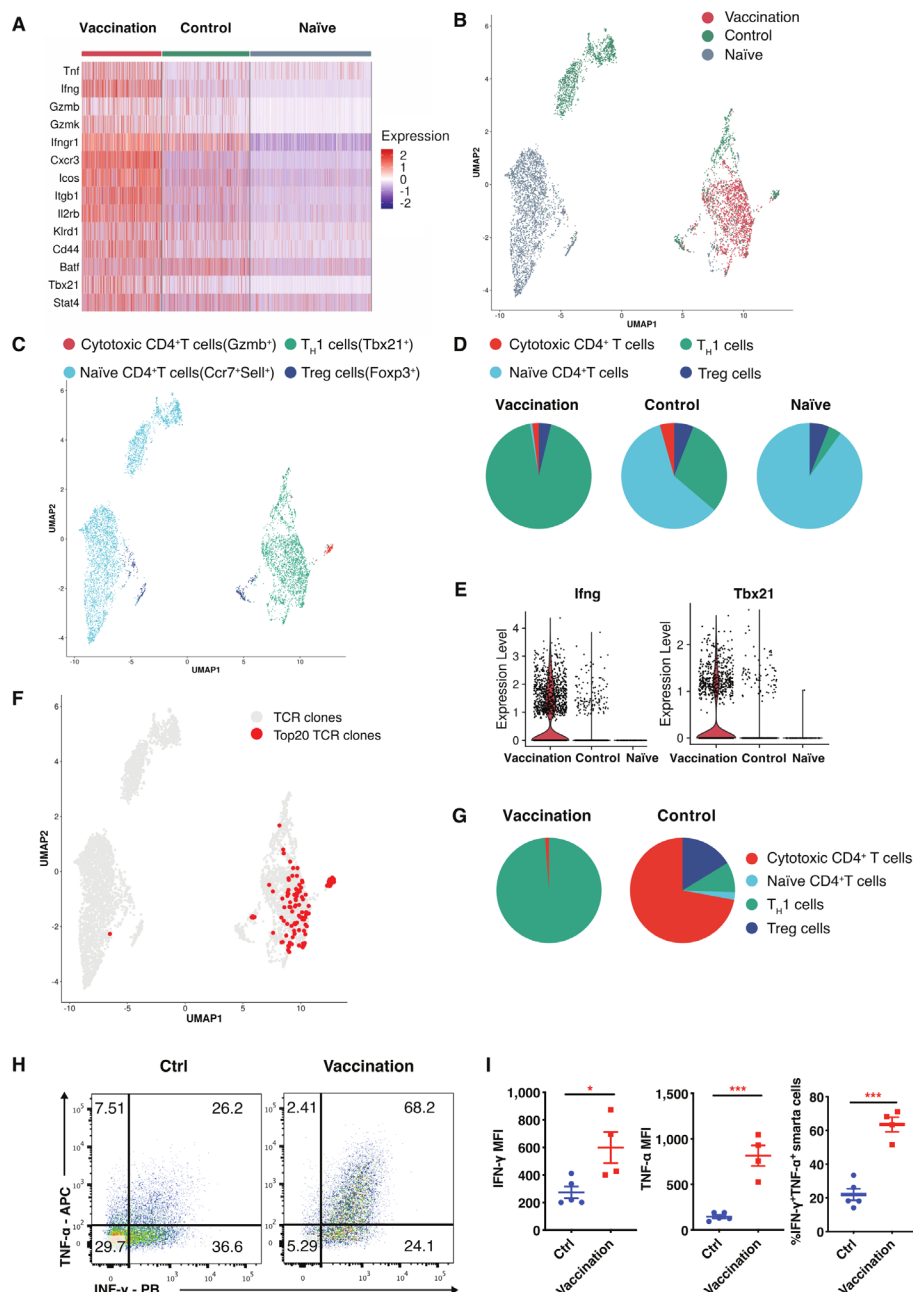
Figure 3 Tumor infiltrating CD4$^+$ T cells induced by the prime-boost vaccination tend to be T$_H$1-polarized. B16-GP tumor-bearing mice received PBS or CD4$^+$ T cell epitope-based heterologous prime-boost vaccination. Afterwards, we sorted CD4$^+$ T cells in tumors from vaccinated (vaccination) and control B16-GP tumor-bearing mice or in lymph nodes from naïve mice (naïve) to perform single-cell RNA sequencing and single-cell TCR sequencing. (A) The heatmap shows differential gene expression of CD4$^+$ T cells in lymph nodes from naïve mice and CD4$^+$ T cells in tumors from control and vaccinated mice. The gene level was scaled to a z-score distribution from –2 to 2. Representative genes for cytokines, surface receptors and transcription factors were listed on the left side of the heatmap. (B) Uniform manifold approximation and projection (UMAP) plot of CD4$^+$ T cells in naïve, control and vaccination groups. Each color represents a different group. (C) Four CD4$^+$ T cells clusters are shown in UMAP plot. Different colors represent cluster origins. Cytotoxic CD4$^+$ T cells; naïve CD4$^+$ T cells; T$_H$1 cells; Treg cells. (D) Pie chart shows the composition of four CD4$^+$ T cells clusters in control, vaccination and naïve groups. (E) The violin plot shows *Ifng and Tbx21* gene expression level in T$_H$1 cells. (F) The TCR clonotypes of CD4$^+$T cells in naïve, control and vaccination groups are shown in UMAP plot. The red one indicates Top20 TCR clones of CD4$^+$ T cells. (G) The top20 clonotypes of CD4$^+$ T cells in naïve, control and vaccination groups distributing in four clusters are shown in the pie chart. (H–I) SMARTA T cells (CD45.1$^+$) were transferred intravenously into B6 mice (CD45.2$^+$) which were bearing 10-day established B16-GP tumors. Cyclophosphamide (CTX) was administered 1 day before T cell transfer. The cytokine production by SMARTA T cells in the tumor of the control and vaccinated mice are represented by flow-cytometry plot (H), INF-γ MFI, TNF-α MFI and the frequency of INF-γ$^+$TNF-α$^+$ SMARTA cells(I) (Ctrl, n=5; vaccination, n=4). Statistical differences (I) are assessed by a two-tailed unpaired Student's t-test. *P<0.05, ***p<0.001. Error bars (I) denote SEM. Data are representation of two independent experiments. TCR, T cell receptor.

Figure 4 CD4^{+} T cell epitope-based heterologous prime-boost vaccination induces strong tumor-specific CD8^{+} T cell response. The vaccination is executed as in figure 1C. Flow cytometry plots for CD44^{hi} staining (A) and CD44^{hi}D^{b}gp$_{33-41}$tetramer^{+} staining (B) gated on CD8^{+} T cells in tumors. The frequency (gated on tumor infiltrating lymphocytes) and number (relative to tumor weight) of total CD44^{hi}CD8^{+} T cells (A) (Ctrl, n=5; Vaccination, n=4) or CD44^{hi}tetramer^{+}CD8^{+} T cells (B) (Ctrl, n=4; vaccination, n=3) of the vaccinated and control mice in tumors (C) On stimulation with LCMV GP$_{33-41}$ peptide and B16F10 GP$_{100}$ peptide (KVPRNQDWL), the cytokine production by CD44^{hi}CD8^{+} T cells in the tumor of the control (n=5) and vaccinated mice (n=7) are shown. Statistical differences (A–C) were assessed by a two-tailed unpaired Student's t-test. *P<0.05, ***p<0.001. Error bars (A–C) denote SEM. Data are representation of two independent experiments.

based on CD4$^+$ T cell epitope was tumor antigen-specific (online supplemental figure 3E).

CD4$^+$ T cell epitope-based heterologous prime-boost vaccination induced polyclonal antitumor CD8$^+$ T cells in TME

To gain more insights into the features of CD8$^+$ T cells induced by prime-boost vaccination with a single CD4$^+$ T cell epitope, we profiled CD8$^+$ T cells in tumors from vaccinated or unvaccinated mice and in lymph nodes from naïve mice by single-cell RNA-sequencing and single-cell TCR-sequencing. We observed that the expression of cytolytic and effector molecules *Gzma*, *Gzmb*, *Gzmk* and *Ifng* was highly enriched in CD8$^+$ T cells from vaccinated mice (figure 5A).

Subclustering of CD8$^+$ T cells revealed the distribution of CD8$^+$ T cells were distinct among these three groups (figure 5B). Recent studies have identified different clusters of exhaustion CD8$^+$ T cell in chronic infection and tumor micro-environment, including progenitor Tex (memory-like Tex cells) cells, transitory Tex cells and terminal Tex cells.[37–41] Memory-like Tex cells replenish transitory Tex and terminal Tex cells and transitory Tex cells possess better effector capacity than terminal Tex cells.[37–41] In total, we defined five clusters of CD8$^+$ T cells based on the unique signature gene profiles. *Tcf-7* was highly enriched in memory-like Tex cells. Transitory Tex cells expressed higher levels of *Cx3cr1* and *Gzmb*, while *Pdcd1* and *Tigit* were highly enriched in Terminal Tex cells. Transitory Tex cells and Terminal Tex cells don't express the gene of *Tcf-7*. Most of the CD8$^+$ T cells were transitory Tex cells and memory-like Tex cells while fewer were terminal Tex cells in tumors from vaccinated mice; in sharp contrast, non-vaccinated mice exhibited the most enriched terminal Tex cells (figure 5C,D). These results suggested that this strategy of vaccination could modulate tumor-reactive CD8$^+$ T cell subsets for better antitumor efficacy.

Furthermore, we observed many of the overall Top20 clonotypes of CD8$^+$ T cells were enriched in TME from vaccinated mice. Even more than 50% of Top20 clonotypes were found to be transitory Tex cells in vaccinated mice, while most of Top20 clonotypes belonged to terminal Tex cells in the tumors of unvaccinated mice (figure 5E,F), which was consistent with the better tumor control in vaccinated mice than in unvaccinated mice. To investigate the specificity of these vaccination induced clonotypes, we blasted the CDR3 sequences with previous data. Three CDR3 sequences of top five clonotypes were mapped to reported TCR sequences specific to B16F10 tumor antigens in vaccinated mice (figure 5G).[46 47] However, in control group, only one CDR3 sequence from top five clonotypes was found to be identical to a reported TCR specific for B16F10 antigen (figure 5H).[46 47] These results illuminated that a single CD4$^+$ T cell epitope based vaccination was able to induce polyclonal antitumor CD8$^+$ T cell responses. To validate this notion, we transplanted the mice with B16-GP tumor cells in one flank, and B16F10 tumor cells in the other

flank followed by sequential LM-GP61 and IAV-GP61 prime-boost vaccination (figure 5I). We found that this vaccination could comparably inhibit the progression of B16F10 tumor and B16-GP tumor in vaccinated mice (figure 5J,K), which corroborated the notion that prime-boost vaccination with a single CD4$^+$ T cell epitope could induce polyclonal antitumor CD8$^+$ T cell response.

Different subsets of dendritic cells (DC) are involved in priming and coordinating antigen-specific CD8$^+$ T cell responses.[18] We compared dendritic cell subsets in TME during prime and boost vaccination. B6 mice were inoculated with B16-GP on Day 0 and then primed with LM-GP61 on Day 5, and a fraction of primed mice were further boosted with IAV-GP61 on day 12. We observed that both the ratio of cDC1 (CD11c^{hi}MHCII^{hi}CD103$^+$CD11b$^-$) to cDC2 (CD11c^{hi}MHCII^{hi}CD103$^-$CD11b$^+$) and the number of cDC1 in tumors were significantly higher in prime/boost vaccination group than those in prime only group or control group, however, the number of cDC2 in tumors had no significant difference among these groups (online supplemental figure 4A,B), demonstrating that the prime-boost vaccination can induce more cDC1 in tumors, which may further improve tumor-specific CD8$^+$ T cell responses given that cDC1 are more specialized in presenting antigens to cognate CD8$^+$ T cells.
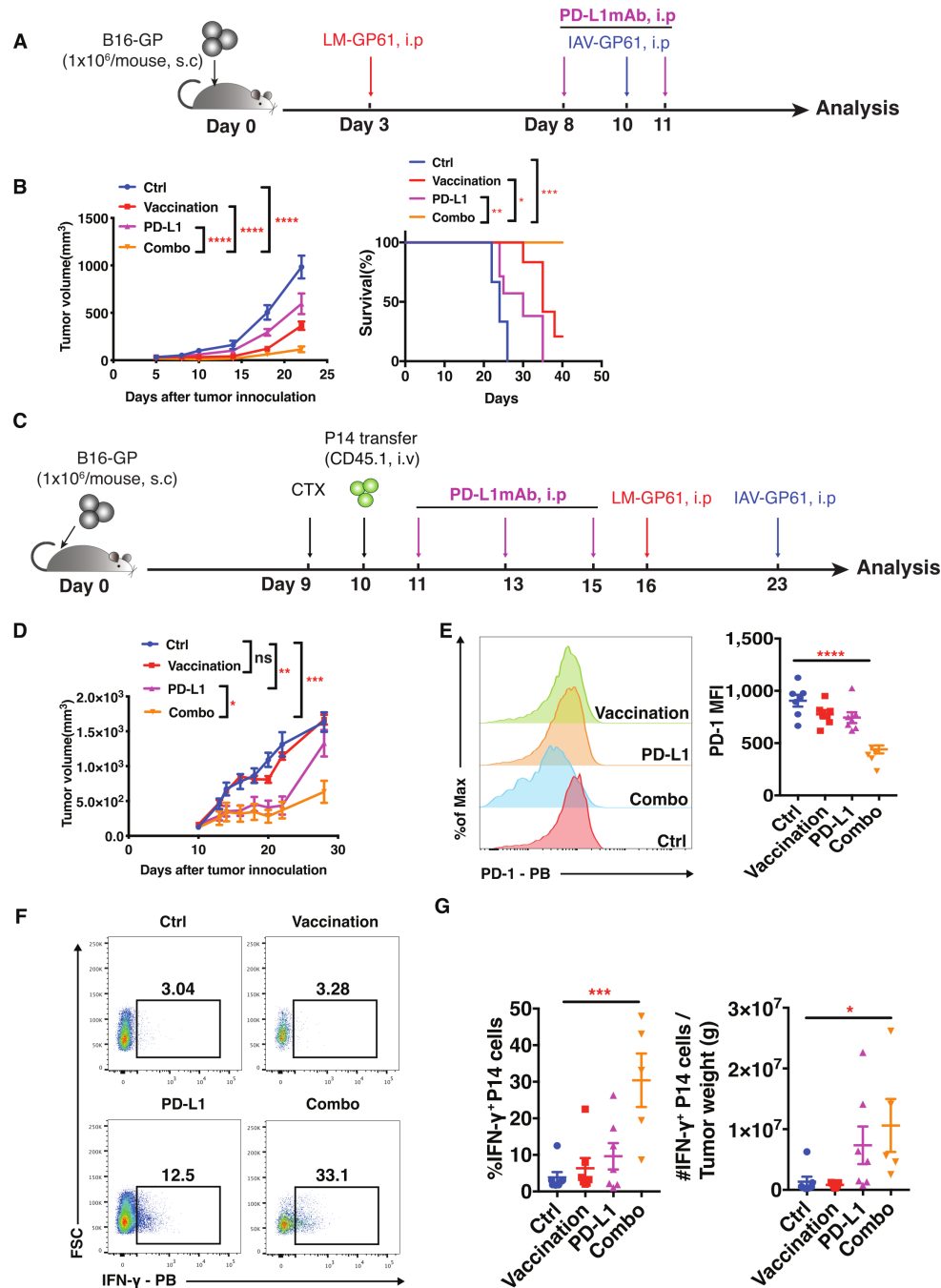
The combination of vaccination and PD-L1 blockade antibody could be more effective than monotherapy

Memory-like Tex cells are thought to respond to PD-1-PD-L1 ICB.[40 41] Since CD4$^+$ T cell epitope-based prime-boost vaccination elicited the increased memory-like Tex population, we next investigated whether this vaccination strategy could synergize with PD-L1 blockade. We found that, compared with PD-L1 ICB only, the combined regimen promoted the efficacy of PD-L1 ICB in suppressing tumor growth and increasing the survival rate (figure 6A,B).

Blocking PD-1 can reinvigorate exhausted CD8$^+$ T cells, however, the reinvigorated CD8$^+$ T cells rapidly become re-exhausted in short time.[48] We next examined whether CD4$^+$ T cell epitope-based prime-boost vaccination could prevent reinvigorated CD8$^+$ T cells from re-exhaustion and then sustain the antitumor efficacy post PD-L1 ICB. Toward this end, we transferred P14 cells into B16-GP melanoma bearing mice which were first received PD-L1 ICB treatment followed by prime-boost vaccination (figure 6C). We found the prime-boost vaccination could effectively sustain the tumor suppression when PD-1 ICB was discontinued, however, in control group, the tumor growth was initially controlled when PD-L1 ICB was present but rapidly resumed after the removal of PD-L1 ICB (figure 6D). This effect could not be attributed to the antitumor effect only mediated by vaccination, given the fact that vaccination only at this extremely late stage (day 16 post-tumor inoculation) failed to repress tumor growth (figure 6D). Consistently, the expression levels of PD-1 on P14 cells were found to be the lowest in the combo group compared with those in other groups (figure 6E) while
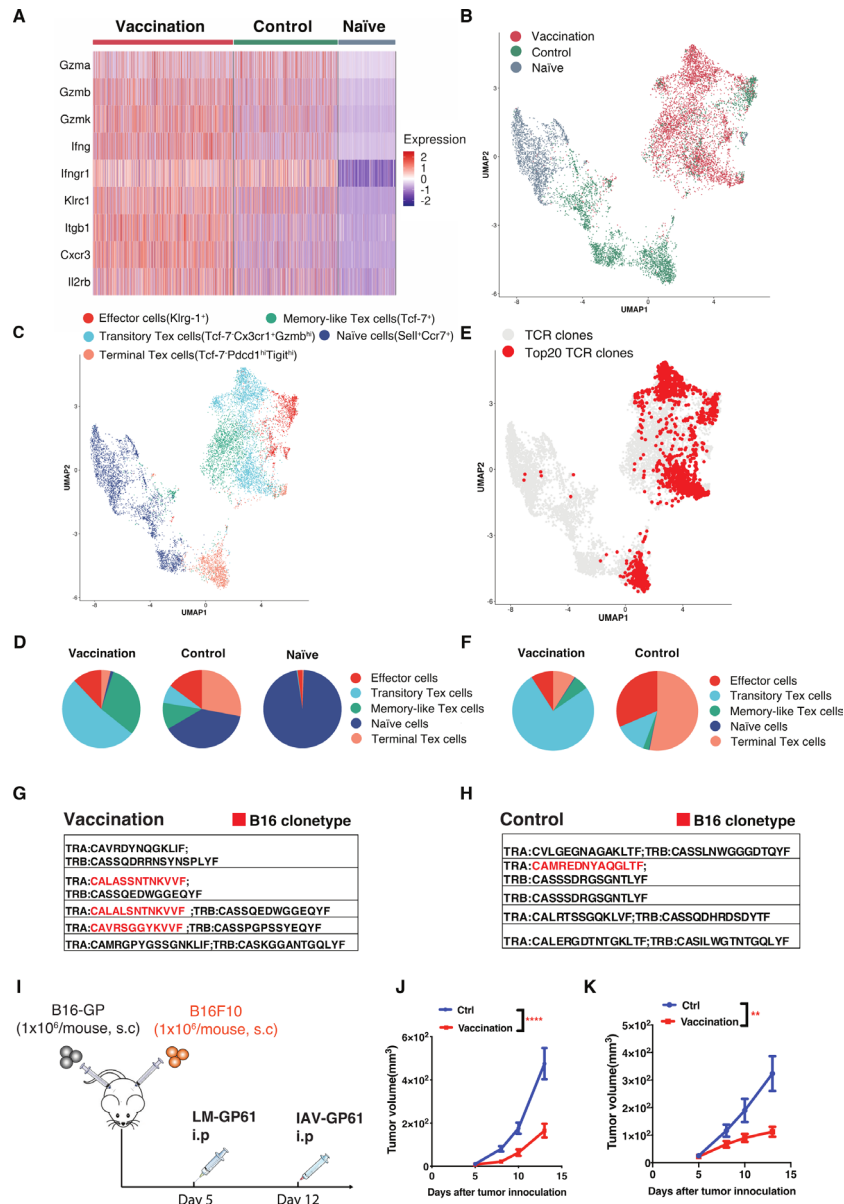
Figure 5 CD4^{+} T cell epitope-based heterologous prime-boost vaccination induces poly-functionality of CD8^{+} T cells. B16-GP tumor-bearing mice received PBS or CD4^{+} T cell epitope-based heterologous prime-boost vaccination. Afterwards, we sorted CD8^{+} T cells in tumors from vaccinated (vaccination) and control B16-GP tumor-bearing mice or in lymph nodes from naïve mice (naïve) to perform single-cell RNA sequencing and single-cell TCR sequencing. (A) Heatmap of relative genes expressed by CD8^{+}T cell from control mice, vaccinated mice and naïve mice. The color indicates the expression level of each gene. Representative genes for cytokine, surface receptors and transcription factors were listed on the left side of the heatmap. (B) Uniform manifold approximation and projection (UMAP) plot of CD8^{+}T cells from control mice, vaccinated mice and naïve mice. The color indicates different group. (C) Five CD8^{+} T cells subsets are shown in uniform manifold approximation and projection (U-MAP) plot. Different colors represent cluster origins. Effector CD8^{+} T cells (Effector cells); Progenitor exhaustion CD8^{+} T cells (memory-like Tex cells); Transitory exhaustion CD8^{+} T cells (Transitory Tex cells); Naïve CD8^{+} T cells (naïve cells); Terminal exhaustion CD8^{+} T cells (Terminal Tex). (D) Pie chart shows the composition of five CD8^{+} T cells clusters in control, vaccination and naïve groups. (E) The TCR clonotypes of CD8^{+} T cells in naïve, control and vaccination groups are shown in UMAP plot. The red one indicates Top20 TCR clones of CD8^{+} T cells. (F) The distributions of the top20 clonotypes of CD8^{+} T cells in control, vaccination and naïve groups are shown in pie chart. (G) The top5 clonotypes CDR3 sequence of CD8^{+} T cells in vaccination group. The red clonotypes symbolize the clonotype CDR3 sequence matched with B16F10 tumor clonotypes CDR3 sequence. (H) The top5 clonotypes CDR3 sequence of CD8^{+} T cells in control group. The red clonotypes symbolize the clonotype CDR3 sequence matched with B16F10 tumor clonotypes CDR3 sequence. (I) B6 mice were transplanted with B16-GP tumor cells (1×10^6 cells/mouse, s.c) in one flank, and with B16F10 tumor cells (1×10^6 cells/mouse, s.c) in the other flank followed by vaccination on day 5 and day 12. The tumor volumes of B16-GP tumors (J) and B16F10 tumors (K) are shown (n=9). Tumor volumes were measured every 3 or 4 days. Statistical significance for tumor growth is determined by two-way ANOVA. **P<0.01, ****p<0.0001. Error bars (J–K) denote SEM. Data are representation of two independent experiments. ANOVA, analysis of variance.

Figure 6 The combination of vaccination and PD-L1 blockade improves antitumor efficacy. (A) Schematic representation of the experimental design. Ctrl indicates mice receiving PBS; PD-L1, PD-L1 mAb treatment; vaccination, immunized by prime-boost vaccination; Combo, the combination of PD-L1 mAb treatment and vaccination. For vaccination and combo group, LM-GP61 (1×10^6 CFU, i.p), IAV-GP61 (0.5 LD50, i.p) were given on day 3 and day 10. For PD-L1 and Combo group, mice were injected intraperitoneally (i.p) with PD-L1 mAb (200 µg/mouse, i.p) on day 8 and day 11. B6 mice were administered with PBS at these four time points as control. (B) Tumor growth curve (Ctrl, n=8; vaccination, n=8; PD-L1, n=9; Combo, n=8) and Kaplan-Meier survival curve (Ctrl, n=5; vaccination, n=5; PD-L1, n=5; Combo, n=5) of mice are shown. Tumor volumes were measured every 3–5 days. (C) Schematic representation of the experimental design. CD45.2$^+$ B6 mice bearing 10-day established B16-GP tumors (1×10^6 cells/mouse, s.c) were received CD45.1$^+$ P14 cells (1×10^6 cells/mouse, intravenously) transfer. Cyclophosphamide (CTX) was administered 1 day before T cell transfer. B6 mice were then administered with PD-L1 mAb (200 µg/mouse, i.p) and vaccination (1×10^6 CFU for LM-GP61 and 0.5 LD50 for IAV-GP61, i.p) at indicated time points. (D) Tumor growth curves (Ctrl, n=5; vaccination, n=7; PD-L1, n=7; Combo, n=6) of mice are shown. Tumor volumes were measured every 2–7 days. PD-1 MFI (E) and the frequency and number of IFN-γ-secreting P14 cells (F–G) in tumors on 14 days post-transfer were determined by FACS (gated on CD45.1$^+$CD8$^+$CD44$^+$ T cells) (n=7, ctrl, vaccination, PD-L1; n=5, Combo). Statistical differences were assessed by ordinary one-way ANOVA analysis (E, G), two-way ANOVA (B, D) and a Mantel-Cox log-rank test for the Kaplan-Meier survival curve (B). *P<0.05, **p<0.01, ***p<0.001, ****p<0.0001, ns stands for not significant. Error bars (B, D, E, G) denote SEM. Data are representation of two (A–G) independent experiments. ANOVA, analysis of variance.

the percentage and number of IFN-γ expressing P14 cells were the highest in the combo group (figure 6F,G). These results revealed that prime-boost vaccination could prevent the re-exhaustion of PD-L1 ICB-reinvigorated CD8+ T cells and sustained the antitumor effects after the cease of PD-L1 ICB. Taken together, these data indicated that CD4+ T cell epitope-based prime-boost vaccination could not only synergize PD-L1 ICB to control the tumor progression but also prolong antitumor effects post the termination of PD-L1 ICB.

DISCUSSION

Cancer therapeutic vaccines are generally targeting MHC-I restricted epitopes to directly induce antitumor cytotoxic CD8+ T cells. Nonetheless, the antitumor response of CD4+ T cells is also very important as tumor-specific CD4+ T cells can eradicate tumors through direct cytolytic activity or helping CD8+ T cells to survive and function in TME.[20 21] Currently, cancer vaccines targeting tumor-specific CD4+ T cell epitopes receive less attention and the underlying mechanisms also remain largely unknown. In this study, we demonstrated a heterologous prime-boost vaccination comprised of Listeria and influenza vectors expressing a single tumor-specific CD4+ T cell epitope, which could effectively restrain tumor growth, reduce tumor metastasis and postsurgery recurrence, and improve overall survival rate in murine tumor models. Furthermore, this CD4+ T cell epitope-based vaccination strategy could synergize and sustain antitumor effects of PD-L1 ICB. Therefore, these findings provide a proof of the concept that therapeutic vaccines targeting tumor-specific CD4+T cell epitopes can effectively inhibit tumor growth, shedding important insights into developing new strategies of antitumor immunotherapy.

In addition to the exogenous CD4+ T cell epitope, we inserted an endogenous CD4+ T cell epitope derived from melanoma tumor-associated antigen tyrosinase related protein (TRP-1) into LM and IAV vectors. It turned out that, endogenous TRP-1$_{106-130}$ CD4+ T cell epitope can indeed induce much comparable tumor growth inhibition as exogenous tumor-specific CD4+ T cell epitopes, suggesting the highly clinical relevance of CD4+ T cell epitope-based vaccination strategy. Moreover, whether endogenous CD4+ T cell epitopes derived from tumor-specific neoantigens have similar antitumor effects warrants further validation.

Tumor-specific T$_H$1 cells are considered as the most critical helper cell subsets in tumor immunity, as these cells could secrete various effector cytokines, including TNF-α and IFN-γ to orchestrate the responses of cytotoxic CD8+ T cells and innate immune cells and activate death receptors on tumor cells. However, during chronical infection and TME, accompanied with CD8+ T cells exhaustion, tumor or virus-specific T$_H$1 cells progressively lose which lead to the disability of virus control and tumor control.[49] Based on this rationale, we employed potent T$_H$1-inducing LM and IVA vectors expressing a single CD4+ T cell epitope

as heterologous prime-boost vaccination strategy. As expected, on vaccination, CD4+ T cells in TME expressed higher levels of T$_H$1 master transcription factor *Tbx21* and secreted T$_H$1 signature cytokines TNF-α and IFN-γ. Moreover, most of the Top20 clonally expanded CD4+ T cells are T$_H$1 cells in vaccination group, indicating prime-boost vaccination can reverse the progressive loss of T$_H$1 and tumor progression.

In relative to cDC2 cells, cDC1 cells play a more important role in cross-presentation of tumor antigens to CD8+ T cells and can also deliver CD4+ T cells help to CD8+ T cells to prime and coordinate antigen-specific CD8+ T cell responses.[50–54] Furthermore, it also has been reported that cDC1 could regulate and drive antitumor CD8+ T cells responses in response to ICB.[55 56] Recent studies have reported a unique memory-like subset of exhausted CD8+ T cells which can proliferate to give rise to transitory and terminal Tex cells. This memory-like Tex subset represents major responders to PD-1-PD-L1 ICB in both chronic viral infection and tumor.[38–41 57] The dendritic cell subset, cDC1, is critical for the differentiation and maintenance of this memory-like Tex subset, potentially by XCL1-XCR1 engagement.[39 57] In line with these notions, our immunization strategy profoundly increased the proportion and number of cDC1 cells. However, the direct evidence demonstrating the important role of cDC1 cells in the antitumor efficacy of CD4+ T cell epitope-based vaccination strategy is lacking, which merits further studies in the future.

Chronical infection and TME can restrain the proliferative capacity and functionality of antiviral and antitumor CD8+ T cells and induce exhaustion CD8+ T cells.[16 17 58] The prime-boost immunization with LM and IAV vectors expressing a single tumor-specific or tumor-associated CD4+ T cell epitope significantly expanded the number and reinvigorated the functionality of exhausted CD8+ T cells in TME. These results also suggested that mice of CD4+ epitope prime-boost immunization likely responded better to PD-1-PD-L1 ICB. As expected, the combination of prime-boost vaccination with PD-L1 ICB exhibited synergized antitumor effects compared with monotherapy. Notably, the vaccination could sustain PD-L1 ICB-reinvigorated exhausted CD8+ T cells by mitigating their re-exhaustion. PD-1-PD-L1 ICB fails to fundamentally alter the exhaustion program of CD8+ T cells due to the fixed epigenetic landscape in exhausted CD8+ T cells.[48 59] It is of great interest to dissect whether CD4+ T cell epitope-based vaccination sustained PD-L1 ICB-reinvigorated CD8+ T cells by inducing any epigenetic changes in these cells.

Notably, we found that the single I-A^b restricted LCMV-GP$_{61-80}$ epitope-based prime-boost immunization induced CD8+ T cell responses not only specific to GP protein but also to non-GP antigens expressed by B16F10 cells, leading to the growth suppression of both B16-GP and B16F10 tumors. One plausible explanation is that GP-specific CD8+ T cells helped by vaccination-induced GP-specific T$_H$1 cells initially mediate tumor cell lysis, resulting

in the efficient release of other non-GP antigens. Furthermore, it is important to continue to investigate whether the vectors expressing multiple tandem tumor-specific CD4$^+$ T cell epitopes are more superior to efficiently induce antitumor immunity.

In conclusion, we have developed a CD4$^+$ T cell epitope-based heterologous immunization strategy that efficiently curtailed tumor progression, metastasis and postsurgery recurrence in preclinical tumor models. Furthermore, this immunization strategy promoted and prolonged PD-1-PD-L1 ICB-mediated antitumor effects. Therefore, the combination of this immunization strategy and PD-1-PD-L1 ICB may represent a novel avenue for cancer immunotherapy.

Author affiliations
[1]Institute of Immunology, Third Military Medical University, Chongqing, China
[2]Department of Dermatology, the Fourth Medical Center, Chinese PLA General Hospital, Beijing, China
[3]Pritzker School of Molecular Engineering, University of Chicago, Chicago, Illinois, USA
[4]Department of Aviation Physiology Training, Qingdao Special Servicemen Recuperation Center of PLA Navy, Qingdao, China
[5]Key Laboratory of Nephrology, Jinling Hospital National Clinical Research Center of Kidney Diseases, Nanjing, Jiangsu, China
[6]Department of Immunology, Huazhong University of Science and Technology Tongji Medical College School of Basic Medicine, Wuhan, Hubei, China
[7]Institute of Cancer, Third Military Medical University Second Affiliated Hospital, Chongqing, China
[8]School of Laboratory Medicine and Biotechnology, Southern Medical University, Guangzhou, Guangdong, China
[9]Guangdong Provincial Key Laboratory of Stomatology, Guanghua School of Stomatology, Stomatological Hospital, Sun Yat-Sen University, Guangzhou, Guangdong, China
[10]Institute of Hepatopancreatobiliary Surgery, Chongqing General Hospital, University of Chinese Academy of Sciences, Chongqing, China
[11]Key Laboratory of Jiangsu Preventive Veterinary Medicine, Key Laboratory for Avian Preventive Medicine, Ministry of Education, College of Veterinary Medicine, Yangzhou University, Yangzhou, Jiangsu, China

Correction notice This article has been updated since it was first published online. The funding statement has been updated.

Contributors LY conceived this study. LY and JH designed the experiments. LXi, MX, SL, ZW, YL, JF, CC performed the experiments. GC analyzed single-cell RNA and TCR sequencing data. LY, LXi, QH, LXu analyzed the data except for single-cell data. JY, PW, XY, JG, SW, ZW, QW, JT, LW, YZ, WY provided reagents, materials and support. LY, LXi, RH, MX, SL, GC prepared the manuscript. LY is responsible for the overall content as the guarantor.

Competing interests The authors declare a conflict of interest. A patent associated with a CD4$^+$ T cell epitope-based therapeutic vaccine has been filed (LY and RH).

Patient consent for publication Not applicable.

Provenance and peer review Not commissioned; externally peer reviewed.

Data availability statement Data are available in a public, open access repository. All data relevant to the study are included in the article or uploaded as online supplemental information. All single-cell RNA-sequencing and single-cell TCR-sequencing data have been deposited in the GEO and are available (GSE175690).

Supplemental material This content has been supplied by the author(s). It has not been vetted by BMJ Publishing Group Limited (BMJ) and may not have been peer-reviewed. Any opinions or recommendations discussed are solely those of the author(s) and are not endorsed by BMJ. BMJ disclaims all liability and

responsibility arising from any reliance placed on the content. Where the content includes any translated material, BMJ does not warrant the accuracy and reliability of the translations (including but not limited to local regulations, clinical guidelines, terminology, drug names and drug dosages), and is not responsible for any error and/or omissions arising from translation and adaptation or otherwise.

ORCID iDs
Jun Huang http://orcid.org/0000-0003-0271-4384
Lilin Ye http://orcid.org/0000-0003-0778-3311

REFERENCES

1 McLane LM, Abdel-Hakeem MS, Wherry EJ. Cd8 T cell exhaustion during chronic viral infection and cancer. *Annu Rev Immunol* 2019;37:457–95.
2 Wherry EJ. T cell exhaustion. *Nat Immunol* 2011;12:492–9.
3 Callahan MK, Postow MA, Wolchok JD. Targeting T cell co-receptors for cancer therapy. *Immunity* 2016;44:1069–78.
4 Ribas A, Wolchok JD. Cancer immunotherapy using checkpoint blockade. *Science* 2018;359:1350–5.
5 Hodi FS, O'Day SJ, McDermott DF, et al. Improved survival with ipilimumab in patients with metastatic melanoma. *N Engl J Med* 2010;363:711–23.
6 Herbst RS, Soria J-C, Kowanetz M, et al. Predictive correlates of response to the anti-PD-L1 antibody MPDL3280A in cancer patients. *Nature* 2014;515:563–7.
7 Robert C, Long GV, Brady B, et al. Nivolumab in previously untreated melanoma without BRAF mutation. *N Engl J Med* 2015;372:320–30.
8 Powles T, Eder JP, Fine GD, et al. MPDL3280A (anti-PD-L1) treatment leads to clinical activity in metastatic bladder cancer. *Nature* 2014;515:558–62.
9 Hargadon KM, Johnson CE, Williams CJ. Immune checkpoint blockade therapy for cancer: an overview of FDA-approved immune checkpoint inhibitors. *Int Immunopharmacol* 2018;62:29–39.
10 Larkin J, Hodi FS, Wolchok JD. Combined nivolumab and ipilimumab or monotherapy in untreated melanoma. *N Engl J Med* 2015;373:1270–1.
11 Motzer RJ, Escudier B, McDermott DF, et al. Nivolumab versus everolimus in advanced renal-cell carcinoma. *N Engl J Med* 2015;373:1803–13.
12 Borghaei H, Paz-Ares L, Horn L, et al. Nivolumab versus docetaxel in advanced Nonsquamous non-small-cell lung cancer. *N Engl J Med* 2015;373:1627–39.
13 Taube JM, Anders RA, Young GD, et al. Colocalization of inflammatory response with B7-H1 expression in human melanocytic lesions supports an adaptive resistance mechanism of immune escape. *Sci Transl Med* 2012;4:127r–37.
14 Spranger S, Spaapen RM, Zha Y. Up-regulation of PD-L1, IDO, and T(regs) in the melanoma tumor microenvironment is driven by CD8(+) T cells. *Sci Transl Med* 2013;5:116r–200.
15 Topalian SL, Drake CG, Pardoll DM. Immune checkpoint blockade: a common denominator approach to cancer therapy. *Cancer Cell* 2015;27:450–61.
16 Wherry EJ, Blattman JN, Murali-Krishna K, et al. Viral persistence alters CD8 T-cell immunodominance and tissue distribution and results in distinct stages of functional impairment. *J Virol* 2003;77:4911–27.
17 Mueller SN, Ahmed R. High antigen levels are the cause of T cell exhaustion during chronic viral infection. *Proc Natl Acad Sci U S A* 2009;106:8623–8.
18 Borst J, Ahrends T, Bąbała N, et al. CD4$^+$ T cell help in cancer immunology and immunotherapy. *Nat Rev Immunol* 2018;18:635–47.
19 Melssen M, Slingluff CL. Vaccines targeting helper T cells for cancer immunotherapy. *Curr Opin Immunol* 2017;47:85–92.
20 Kennedy R, Celis E. Multiple roles for CD4+ T cells in anti-tumor immune responses. *Immunol Rev* 2008;222:129–44.
21 Marzo AL, Kinnear BF, Lake RA, et al. Tumor-specific CD4+ T cells have a major "post-licensing" role in CTL mediated anti-tumor immunity. *J Immunol* 2000;165:6047–55.
22 Fearon ER, Pardoll DM, Itaya T, et al. Interleukin-2 production by tumor cells bypasses T helper function in the generation of an antitumor response. *Cell* 1990;60:397–403.

23 Zajac AJ, Blattman JN, Murali-Krishna K, *et al*. Viral immune evasion due to persistence of activated T cells without effector function. *J Exp Med* 1998;188:2205–13.

24 Kurts C, Carbone FR, Barnden M, *et al*. Cd4+ T cell help impairs CD8+ T cell deletion induced by cross-presentation of self-antigens and favors autoimmunity. *J Exp Med* 1997;186:2057–62.

25 Bennett SR, Carbone FR, Karamalis F, *et al*. Help for cytotoxic-T-cell responses is mediated by CD40 signalling. *Nature* 1998;393:478–80.

26 Schoenberger SP, Toes RE, van der Voort EI, *et al*. T-cell help for cytotoxic T lymphocytes is mediated by CD40-CD40L interactions. *Nature* 1998;393:480–3.

27 Ridge JP, Di Rosa F, Matzinger P. A conditioned dendritic cell can be a temporal bridge between a CD4+ T-helper and a T-killer cell. *Nature* 1998;393:474–8.

28 Nakanishi Y, Lu B, Gerard C, *et al*. CD8(+) T lymphocyte mobilization to virus-infected tissue requires CD4(+) T-cell help. *Nature* 2009;462:510–3.

29 Bos R, Sherman LA. CD4+ T-cell help in the tumor milieu is required for recruitment and cytolytic function of CD8+ T lymphocytes. *Cancer Res* 2010;70:8368–77.

30 Ahrends T, Spanjaard A, Pilzecker B, *et al*. CD4+T Cell Help Confers a Cytotoxic T Cell Effector Program Including Coinhibitory Receptor Downregulation and Increased Tissue Invasiveness. *Immunity* 2017;47:848–61.

31 He R, Yang X, Liu C, *et al*. Efficient control of chronic LCMV infection by a CD4 T cell epitope-based heterologous prime-boost vaccination in a murine model. *Cell Mol Immunol* 2018;15:815–26.

32 San Mateo LR, Chua MM, Weiss SR, *et al*. Perforin-mediated CTL cytolysis counteracts direct cell-cell spread of Listeria monocytogenes. *J Immunol* 2002;169:5202–8.

33 Szretter KJ, Balish AL, Katz JM. Influenza: propagation, quantification, and storage. *Curr Protoc Microbiol* 2006;Chapter 15:Chapter 15:Unit 15G 1.

34 Akbay EA, Koyama S, Liu Y, *et al*. Interleukin-17A promotes lung tumor progression through neutrophil attraction to tumor sites and mediating resistance to PD-1 blockade. *J Thorac Oncol* 2017;12:1268–79.

35 Li Y, Wang Z, Lin H, *et al*. Bcl6 preserves the suppressive function of regulatory T cells during tumorigenesis. *Front Immunol* 2020;11:806.

36 Stuart T, Butler A, Hoffman P, *et al*. Comprehensive integration of single-cell data. *Cell* 2019;177:1888–902.

37 Hudson WH, Gensheimer J, Hashimoto M, *et al*. Proliferating Transitory T Cells with an Effector-like Transcriptional Signature Emerge from PD-1+ Stem-like CD8+ T Cells during Chronic Infection. *Immunity* 2019;51:1043–58.

38 He R, Hou S, Liu C, *et al*. Follicular CXCR5- expressing CD8(+) T cells curtail chronic viral infection. *Nature* 2016;537:412–28.

39 Im SJ, Hashimoto M, Gerner MY, *et al*. Defining CD8+ T cells that provide the proliferative burst after PD-1 therapy. *Nature* 2016;537:417–21.

40 Siddiqui I, Schaeuble K, Chennupati V, *et al*. Intratumoral Tcf1+PD-1+CD8+T Cells with Stem-like Properties Promote Tumor Control in Response to Vaccination and Checkpoint Blockade Immunotherapy. *Immunity* 2019;50:195–211.

41 Kurtulus S, Madi A, Escobar G, *et al*. Checkpoint Blockade Immunotherapy Induces Dynamic Changes in PD-1−CD8+ Tumor−Infiltrating T Cells. *Immunity* 2019;50:181–94.

42 Pan ZK, Ikonomidis G, Lazenby A, *et al*. A recombinant Listeria monocytogenes vaccine expressing a model tumour antigen protects mice against lethal tumour cell challenge and causes regression of established tumours. *Nat Med* 1995;1:471–7.

43 Shen H, Slifka MK, Matloubian M, *et al*. Recombinant Listeria monocytogenes as a live vaccine vehicle for the induction of protective anti-viral cell-mediated immunity. *Proc Natl Acad Sci U S A* 1995;92:3987–91.

44 Restifo NP, Surman DR, Zheng H, *et al*. Transfectant influenza A viruses are effective recombinant immunogens in the treatment of experimental cancer. *Virology* 1998;249:89–97.

45 Rodrigues M, Li S, Murata K, *et al*. Influenza and vaccinia viruses expressing malaria CD8+ T and B cell epitopes. Comparison of their immunogenicity and capacity to induce protective immunity. *J Immunol* 1994;153:4636–48.

46 Carmona SJ, Siddiqui I, Bilous M, *et al*. Deciphering the transcriptomic landscape of tumor-infiltrating CD8 lymphocytes in B16 melanoma tumors with single-cell RNA-seq. *Oncoimmunology* 2020;9:1737369.

47 Chang YM, Wieland A, Li Z-R, *et al*. T cell receptor diversity and lineage relationship between virus-specific CD8 T cell subsets during chronic lymphocytic choriomeningitis virus infection. *J Virol* 2020;94. doi:10.1128/JVI.00935-20. [Epub ahead of print: 29 09 2020].

48 Pauken KE, Sammons MA, Odorizzi PM, *et al*. Epigenetic stability of exhausted T cells limits durability of reinvigoration by PD-1 blockade. *Science* 2016;354:1160–5.

49 Snell LM, Osokine I, Yamada DH, *et al*. Overcoming CD4 Th1 Cell Fate Restrictions to Sustain Antiviral CD8 T Cells and Control Persistent Virus Infection. *Cell Rep* 2016;16:3286–96.

50 Eickhoff S, Brewitz A, Gerner MY, *et al*. Robust anti-viral immunity requires multiple distinct T Cell-Dendritic cell interactions. *Cell* 2015;162:1322–37.

51 Hor JL, Whitney PG, Zaid A, *et al*. Spatiotemporally distinct interactions with dendritic cell subsets facilitates CD4+ and CD8+ T cell activation to localized viral infection. *Immunity* 2015;43:554–65.

52 Bachem A, Güttler S, Hartung E, *et al*. Superior antigen cross-presentation and XCR1 expression define human CD11c+CD141+ cells as homologues of mouse CD8+ dendritic cells. *J Exp Med* 2010;207:1273–81.

53 Joffre OP, Segura E, Savina A, *et al*. Cross-presentation by dendritic cells. *Nat Rev Immunol* 2012;12:557–69.

54 Eisenbarth SC. Dendritic cell subsets in T cell programming: location dictates function. *Nat Rev Immunol* 2019;19:89–103.

55 Mayoux M, Roller A, Pulko V, *et al*. Dendritic cells dictate responses to PD-L1 blockade cancer immunotherapy. *Sci Transl Med* 2020;12. doi:10.1126/scitranslmed.aav7431. [Epub ahead of print: 11 03 2020].

56 Salmon H, Idoyaga J, Rahman A, *et al*. Expansion and Activation of CD103(+) Dendritic Cell Progenitors at the Tumor Site Enhances Tumor Responses to Therapeutic PD-L1 and BRAF Inhibition. *Immunity* 2016;44:924–38.

57 Schenkel JM, Herbst RH, Canner D, *et al*. Conventional type I dendritic cells maintain a reservoir of proliferative tumor-antigen specific TCF-1+ CD8+ T cells in tumor-draining lymph nodes. *Immunity* 2021;54:2338–53.

58 Wherry EJ, Kurachi M. Molecular and cellular insights into T cell exhaustion. *Nat Rev Immunol* 2015;15:486–99.

59 Sen DR, Kaminski J, Barnitz RA, *et al*. The epigenetic landscape of T cell exhaustion. *Science* 2016;354:1165–9.